Front. Phys. China
DOI 10.1007/s11467-009-0077-8

RESEARCH ARTICLE

Low-energy Ce spin excitations in CeFeAsO and $CeFeAsO_{0.84}F_{0.16}$

Shi-liang LI (李世亮)[1,2], **Dao-xin YAO** (姚道新)[3], **Yi-ming QIU** (邱义铭)[4,5], **Hye Jung KANG**[6], **E. W. CARLSON**[3], **Jiang-ping HU** (胡江平)[3], **Gen-fu CHEN** (陈根富)[7], **Nan-lin WANG** (王楠林)[1], **Peng-cheng DAI** (戴鹏程)[2,8,1](✉)

[1] *Beijing National Laboratory for Condensed Matter Physics, Institute of Physics, Chinese Academy of Sciences, Beijing 100190, China*
[2] *Department of Physics and Astronomy, The University of Tennessee, Knoxville, TN 37996-1200, USA*
[3] *Department of Physics, Purdue University, West Lafayette, IN 47907, USA*
[4] *NIST Center for Neutron Research, National Institute of Standards and Technology, Gaithersburg, MD 20899, USA*
[5] *Department of Materials Science and Engineering, University of Maryland, College Park, MD 20742, USA*
[6] *Department of Physics and Astronomy, Clemson University, Clemson, SC 29634, USA*
[7] *Department of Phyiscs, Renmin University of China, Beijing 100872, China*
[8] *Neutron Scattering Sciences Division, Oak Ridge National Laboratory, Oak Ridge, TN 37831-6393, USA*
E-mail: laoliang@gmail.com, daip@ornl.gov

Received September 14, 2009; accepted September 30, 2009

We use inelastic neutron scattering to study the low-energy spin excitations of polycrystalline samples of nonsuperconducting CeFeAsO and superconducting $CeFeAsO_{0.84}F_{0.16}$. Two sharp dispersionless modes are found at 0.85 and 1.16 meV in CeFeAsO below the Ce antiferromagnetic (AF) ordering temperature of $T_N^{Ce} \sim 4$ K. On warming to above $T_N^{Ce} \sim 4$ K, these two modes become one broad dispersionless mode that disappears just above the Fe ordering temperature $T_N^{Fe} \sim 140$ K. For superconducting $CeFeAsO_{0.84}F_{0.16}$, where Fe static AF order is suppressed, we find a weakly dispersive mode center at 0.4 meV that may arise from short-range Ce–Ce exchange interactions. Using a Heisenberg model, we simulate powder-averaged Ce spin wave excitations. Our results show that we need both Ce spin wave and crystal electric field excitations to account for the whole spectra of low-energy spin excitations.

Keywords iron pnictides, rare earth spin waves, crystal field

PACS numbers 71.70.Ch, 75.30.Ds, 74.25.Ha

The parent compounds of iron arsenide superconductors such as RFeAsO (R =La, Ce, Nd, Sm, Pr, ...) are long-range ordered antiferromagnets where iron spins form a collinear antiferromagnetic (AF) structure [1–8]. Although a lot of efforts over the past year have focused on the magnetism from iron 3d electrons, the interplay between the iron 3d and rare earth 4f electrons in iron oxypnictides may also play an important role in determining the electronic properties of these materials. For example, while LaFePO is a low-temperature bulk superconductor [9], CeFePO exhibits heavy fermion behavior with a Kondo temperature $T_K \approx 10$ K [10]. For the undoped CeFeAsO, Ce f-electrons order antiferromagnetically at $T_N^{Ce} \approx 4$ K [5] with no signature of heavy fermion behavior. Theoretically, the 3d–4f hybridization is found to be different between CeFePO and CeFeAsO by LDA+DMFT calculation [11]. The Kondo screening of the f-moments may be efficiently suppressed by the d-electron ordering [12]. The zero field muon spin relaxation (μsR) measurement has indeed found a strong Fe–Ce coupling in CFAO that results in a large staggered Ce magnetization induced by the magnetically ordered Fe sublattice far above T_N^{Ce} [13]. A recent neutron diffraction study on the $CeFeAs_{1-x}P_xO$ further reveals a lattice distortion induced magnetic quantum phase transition where the AF orders of Fe 3d and Ce 4f electrons are suppressed upon substitution of P for As [14].

To understand the magnetic interaction between 3d and 4f electrons in CeFeAsO and its electron-doped superconductor $CeFeAsO_{1-x}F_x$, we carried out inelastic neutron scattering studies on the low energy spin excitations in polycrystalline CeFeAsO and $CeFeAsO_{0.84}F_{0.16}$. We observe clear Ce spin waves below T_N^{Ce} in CeFeAsO and can model them using a Heisenberg model. However,

we also need to include the Ce crystalline electric field (CEF) excitations in order to understand the observed excitation spectra [15]. Ce spin excitations are also found in the superconducting $CeFeAsO_{0.84}F_{0.16}$ sample.

We grew polycrystalline non-superconducting CeFeAsO and superconducting $CeFeAsO_{0.84}F_{0.16}$ with $T_c = 41$ K using the method described elsewhere [3]. The non-superconducting LaFeAsO (LFAO) sample was also prepared by the same method to isolate the magnetic scattering from Ce in CeFeAsO since La^{3+} is nonmagnetic. The inelastic neutron scattering measurements were performed on the Disk Chopper Spectrometer (DCS) and Spin-Polarized Triple-Axis Spectrometer (SPINS) at the NIST Center for Neutron Research (NCNR). We choose orthorhombic *Cmma* space group to describe the magnetic structure of Ce spins in CeFeAsO, whose unit cell can be indexed as $\sqrt{2}a_N \times \sqrt{2}b_N \times 2c_N$ where a_N, b_N and c_N are nuclear lattice constants [5].

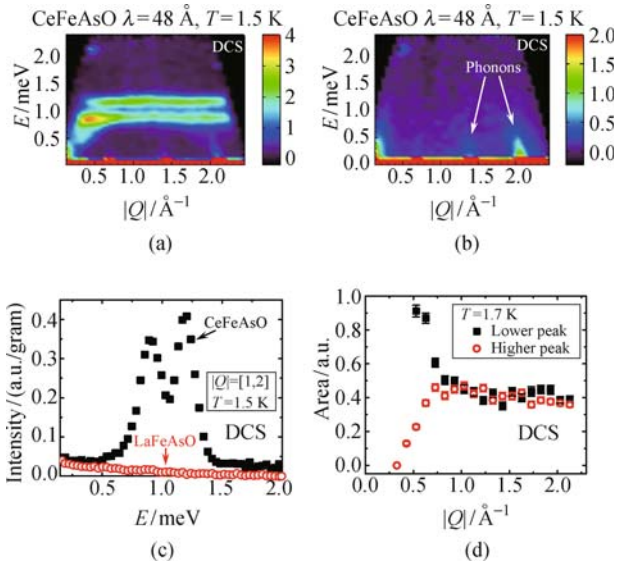

Fig. 1 **(a)** 2-D mapping of spin excitations of CeFeAsO at $T = 1.5$ K. There are two sharp dispersionless modes at 1.2 meV and 0.9 meV respectively. **(b)** Same measurement on LFAO as that in **(a)**. No spin excitation is observable. A comparison of energy cuts with $|Q|$ integrated from 1 to 2 Å^{-1} between these two systems is given in **(c)**. **(d)** The integrated intensities of two peaks at different $|Q|$. Error bars in all figs represent $\pm 1\sigma$.

We begin by showing the Ce magnetic excitations at 1.5 K, a temperature well below T_N^{Ce}, in Fig. 1(a). One can see clear acoustic spin waves dispersing from $|Q| \sim 0.36$ Å^{-1}, which corresponds to $(0, 0, 1)_M$ AF ordering wave vector of Ce. There is a small spin gap (~ 0.3 meV) usually arising from the anisotropy effect [16, 17]. The most prominent features in Fig. 1(a) are two sharp dispersionless modes at ∼1.2 meV and 0.9 meV. Detailed cuts suggest that the intensities of both modes show little change for $|Q| > 0.8$ Å^{-1}, as shown in Fig. 1(d). Since such a mode is not observed in LaFeAsO [Fig. 1(c)], the observed two weakly dispersive modes must arise from Ce unpaired 4f electrons.

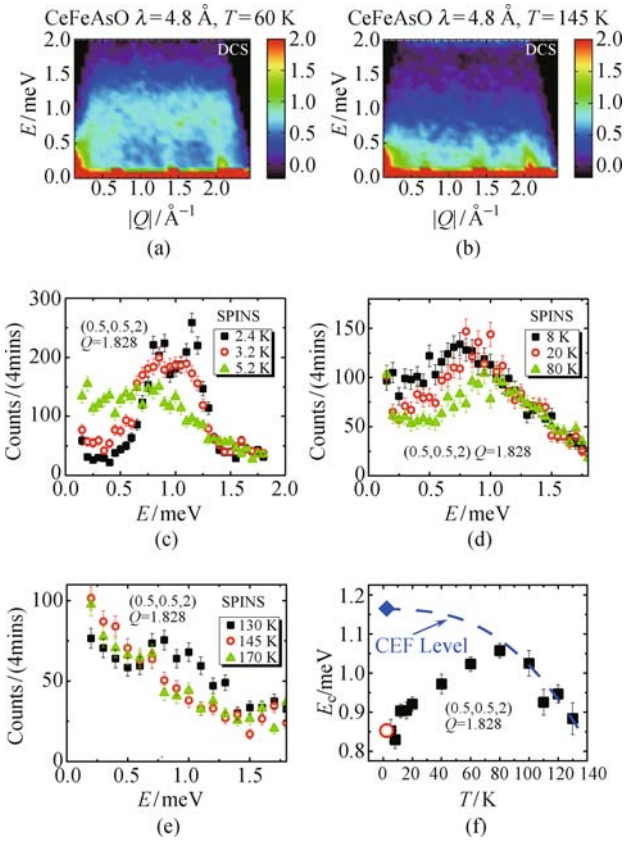

Fig. 2 **(a)** 2-D mapping of spin excitations of CFAO at $T = 60$ K, where two sharp dispersionless modes at low temperature become one broad mode. This mode disappears above T_N^{Fe}, as shown in **(b)**. **(c)**–**(e)** The temperature dependence at $|Q| = 1.818$ Å^{-1}. **(f)** The temperature dependence of centers of these modes.

Above T_N^{Ce}, the acoustic spin waves disappear as expected. The two dispersionless modes change to one broad dispersionless mode with a typical energy full width at half maximum (FWHM) of ~ 0.75 meV, much larger than the energy resolution (~ 0.1 meV) as shown in Fig. 2(a). Above the Fe ordering temperature T_N^{Fe}, the mode disappears and the low energy excitations show quasi-elastic paramagnetic scattering, as shown in Fig. 2(b). To study the detailed temperature evolution of this mode, we carried out energy scans at $|Q| = 1.828$ Å^{-1} at SPINS. Figure 2(c) shows that the two sharp modes become one broad mode right above T_N^{Ce}. Further increasing temperature results in a shift of the mode to higher energy, as shown in Fig. 2(d). The intensities above 1 meV actually show no change with increasing temperature and it is the intensity loss at low energies that leads to the shift of the mode. Figure 2(e) shows that the mode disappears above T_N^{Fe}. In Fig. 2(f), we give the temperature dependence of the center of the mode. The circle and diamond symbols are the fitting results of two peaks at 2.4 K.

In order to model the magnetic excitations at low temperature, we use a Heisenberg model to describe the exchange interactions between local moments:

$$
\begin{aligned}
H = {} & J_{1x}\sum_{\boldsymbol{r}} \boldsymbol{S}^{\mathrm{Fe}}_{\boldsymbol{r}} \cdot \boldsymbol{S}^{\mathrm{Fe}}_{\boldsymbol{r}+\boldsymbol{a}} + J_{1y}\sum_{\boldsymbol{r}} \boldsymbol{S}^{\mathrm{Fe}}_{\boldsymbol{r}} \cdot \boldsymbol{S}^{\mathrm{Fe}}_{\boldsymbol{r}+\boldsymbol{b}} \\
& + J_2 \sum_{\boldsymbol{r}} \boldsymbol{S}^{\mathrm{Fe}}_{\boldsymbol{r}} \cdot (\boldsymbol{S}^{\mathrm{Fe}}_{\boldsymbol{r}+\boldsymbol{a}+\boldsymbol{b}} + \boldsymbol{S}^{\mathrm{Fe}}_{\boldsymbol{r}+\boldsymbol{a}-\boldsymbol{b}}) + J_z \sum_{\boldsymbol{r}} \boldsymbol{S}^{\mathrm{Fe}}_{\boldsymbol{r}} \cdot \boldsymbol{S}^{\mathrm{Fe}}_{\boldsymbol{r}+\boldsymbol{c}} \\
& + J_c \sum_{\boldsymbol{r},\boldsymbol{\delta}\neq\boldsymbol{\delta}'} \boldsymbol{S}^{\mathrm{Ce}}_{\boldsymbol{r}+\frac{1}{2}\boldsymbol{c}+\boldsymbol{\delta}} \cdot \boldsymbol{S}^{\mathrm{Ce}}_{\boldsymbol{r}+\frac{1}{2}\boldsymbol{c}+\boldsymbol{\delta}'} + J_{zc}\sum_{\boldsymbol{r},\boldsymbol{\delta}} \boldsymbol{S}^{\mathrm{Ce}}_{\boldsymbol{r}+\frac{1}{2}\boldsymbol{c}+\boldsymbol{\delta}} \cdot \boldsymbol{S}^{\mathrm{Ce}}_{\boldsymbol{r}-\frac{1}{2}\boldsymbol{c}+\boldsymbol{\delta}} \\
& + J_{cf}\sum_{\boldsymbol{r}} (S^{\mathrm{Ce}}_{\boldsymbol{r}+\frac{1}{2}\boldsymbol{c}+\boldsymbol{\delta}_1} \cdot S^{\mathrm{Fe}}_{\boldsymbol{r}} + S^{\mathrm{Ce}}_{\boldsymbol{r}+\frac{1}{2}\boldsymbol{c}+\boldsymbol{\delta}_3} \cdot S^{\mathrm{Fe}}_{\boldsymbol{r}}) + J_{cf}\sum_{\boldsymbol{r}} (S^{\mathrm{Ce}}_{\boldsymbol{r}-\frac{1}{2}\boldsymbol{c}+\boldsymbol{\delta}_2} \cdot S^{\mathrm{Fe}}_{\boldsymbol{r}} + S^{\mathrm{Ce}}_{\boldsymbol{r}-\frac{1}{2}\boldsymbol{c}+\boldsymbol{\delta}_4} \cdot S^{\mathrm{Fe}}_{\boldsymbol{r}})
\end{aligned} \tag{1}
$$

where $\boldsymbol{r}$ denotes the positions of Fe atoms. The vector connecting Fe atoms in the $\hat{x}$ direction is $\boldsymbol{a}$, while that connecting Fe in the $\hat{y}$ direction is $\boldsymbol{b}$. The vector from one Fe layer to the next is $\boldsymbol{c}$. The vectors δ represent the relative positions of the Ce and O atoms.

The coupling constants are represented in Fig. 3(a). We take the coupling between nearest-neighbor Fe atoms to be antiferromagnetic (J_{1x}) and ferromagnetic (J_{1y}) respectively as reported in $CaFe_2As_2$ [18]. The coupling between next-nearest Fe atoms, J_2, is taken to be antiferromagnetic. We note that the low energy scale of Ce spin excitations is basically determined by the couplings related to Ce, so the values of J_1 and J_2 have insignificant effects on the final results. We assume a weak ferromagnetic coupling J_z between Fe atoms along the c axis. In addition, we assume that the Ce moments are highly localized and weakly coupled as one would expect for f-electron system. Based on the powder diffraction results, the Ce atoms have a weak in-plane ferromagnetic moment, which alternates from plane to plane, and is responsible for doubling the unit cell in the c-direction. In deriving the spin structure factor, we have taken this component [i.e. the $(0,\ 0,\ 1)_M$ component] to be collinear with the Fe ordering, and neglected the $(1,\ 0,\ 0)_M$ component of the Ce order for simplicity. The coupling between Ce atoms within the same Ce–O plane J_c is assumed to be ferromagnetic, but the coupling between Ce atoms in different planes J_{zc} is antiferromagnetic. We also include the effects of frustration between the Ce and Fe atoms. Note that the coupling between the Fe and Ce systems is highly frustrated. This is because a Ce atom which sits on, e.g., the top of a Ce–O layer couples to four Fe atoms in the nearest neighbor Fe–As layer above it. Since the Fe atoms have an antiferromagnetic order, the Ce–Fe interaction is completely frustrated, regardless of the sign of the Ce–Fe coupling, J_{cf}.

We use linearized spin wave theory to calculate the dynamic structure factor [19]

$$
S(\boldsymbol{k},\omega) = \sum_f \sum_{i=x,y,z} |\left\langle f|S^i(\boldsymbol{k})|0\right\rangle|^2 \delta(\omega-\omega_f) \tag{2}
$$

where $|0\rangle$ is the magnon vacuum state and $|f\rangle$ denotes the final state of the spin system with excitation energy ω_f. The angle-average of $S(\boldsymbol{k},\omega)$ is proportional to the expected powder-averaged neutron scattering intensity.

Figure 3(b) and (c) give our calculated results for powder-averaged low-temperature magnetic excitations when both Fe and Ce spins are ordered and only Ce spins are ordered respectively. Our calculation successfully reproduces the low Q acoustic spin wave starting from $(0,\ 0,\ 1)_M$ and the high Q dispersionless characteristic of the magnetic excitations. Comparing Fig. 3(b) and (c) shows that couplings between Ce–Fe spins have little effect on the Ce spin waves since they are frustrated. In addition, the values of Fe–Fe couplings also make little contribution to the Ce spin waves due to their large values.

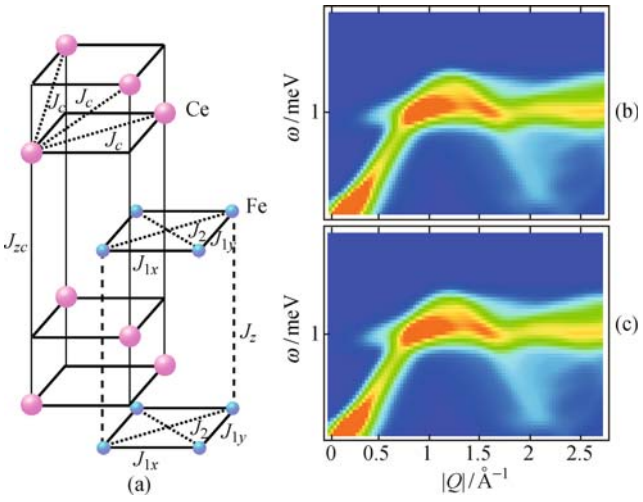

Fig. 3 **(a)** Effective couplings between magnetic moments, as described in the text. **(b)** Angle-average of the spin structure factor when both Fe and Ce spins are ordered at low temperature. Here, we have used $J_{1x} = 49.9$, $J_{1y} = -5.7$, $J_2 = 18.9$, $J_z = -0.01$, $J_c = -0.1$, $J_{zc} = 0.02$ and $J_{cf} = 0.5$ meV. **(c)** Angle-average of the spin structure factor when only Ce spins order at low tcemperature. All the Fe–Fe coupling and Fe–Ce coupling are set to zero. The frequency is in units of $J_2 S^{\mathrm{Fe}}_z$, and we have used the measured ratio of $S^{\mathrm{Ce}}_z/S^{\mathrm{Fe}}_z \sim 1.1$.

Although this model can explain the dispersive spin waves from Ce AF ordering wavevector, it fails to explain the two dispersionless modes existing below T_N^{Ce}. To understand our data, we note that AF ordering in CeFeAsO can split the Ce CEF levels [15]. At a temperature above T_N^{Ce} but below T_N^{Fe}, a broad peak can come from the split of low-energy CEF level. At low temperature, the ordered Ce spins produce the lower branch of the modes, but the higher branch is still related to

CEF. The observed small ordered Ce moment [5] is consistent with this picture. Above $T_N^{\rm Ce}$, the Ce spin fluctuations persist at lower energies due to the coupling between Fe and Ce moments [13] while the CEF level is still above 1 meV, which explains the large FWHM of the mode. The remaining short-range coupling between Fe and Ce moments may be non-Heisenberg-type [13], or the Heisenberg fluctuations at finite frequency despite of the frustration in the zero-frequency limit. Increasing temperature up to $T_N^{\rm Fe}/2$ only reduces the intensities at low energies [Fig. 2(d)] while the CEF level shows little change [Fig. 2(f)]. This picture suggests that the Ce 4f-electrons can be coupled to Fe 3d-electrons via a local-moment-like picture at low energies or through CEF.

We now turn to the superconducting $CeFeAsO_{0.84}F_{0.16}$, where similar measurements on DCS were performed. Fig. 4(a) shows the presence of the acoustic spin wave dispersing from $(0, 0, 1)_M$. This is consistent with a short-range ordering of Ce moment at low temperature, as shown in Fig. 4(b). The correlation length is about 32 Å by fitting the data with Gaussian lineshape. Figure 4(c) gives a direct comparison between superconducting $CeFeAsO_{0.84}F_{0.16}$ and nonsuperconducting LaFeAsO, which clearly shows the presence of a dispersionless mode at energy $\sim$ 0.6 meV. With increasing temperature, the intensity of the mode quickly drops and the mode faintly disappears above $T \sim 15$ K, as shown in Fig. 4(d). Since there is no CEF splitting due to the absence of long-range Fe AF order in superconducting sample [15], this mode is only related to Ce spin–spin correlations. In $CeFeAs_{1-x}P_xO$ system, Ce ordering vanishes well before the disappearance of Fe ordering [14], which suggests that the Ce–Ce coupling itself is very weak. It is thus possible that the mode in the superconducting sample is related to the Fe spin fluctuations.

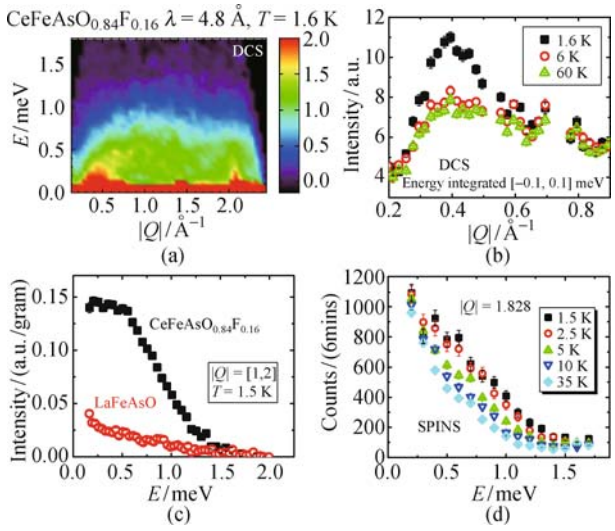

Fig. 4 **(a)** 2-D mapping of spin excitations of superconducting CFAOF (x=0.16) at $T = 1.6$ K. **(b)** Short-range order of Ce spins around $Q = (0, 0, 1)_M$. **(c)** Energy cut with $|Q|$ integrated from 1 to 2 Å^{-1}. (d) Temperature dependence of the dispersionless mode.

In conclusion, we have studied the low energy spin excitations in polycrystalline CeFeAsO. We report the acoustic spin wave dispersing from $(0, 0, 1)_M$ and simulate the results using a simple Heisenberg Hamiltonian. We also observe two distinct dispersionless modes below $T_N^{\rm Ce}$, which become one broad mode with increasing temperature. Our results suggest that a combination of the effects from both the direct Fe–Ce coupling and the Ce CEF split due to Fe ordering is needed to understand the interplay of 4f–3d electrons. For superconducting $CeFeAsO_{0.84}F_{0.16}$, we find a broad mode at low temperature suggesting Ce–Ce short-range spin correlations.

Acknowledgements This work was supported by the US Department of Energy, Division of Materials Science, Basic Energy Sciences, through DOE DE-FG02-05ER46202. The work at the Institute of Physics, Chinese Academy of Sciences, was supported by the Chinese Academy of Sciences. Work at NCNR was in part supported by the National Science Foundation under agreement DMR-0454672.

References

1. Y. Kamihara, T. Watanabe, M. Hirano, and H. Hosono, J. Am. Chem. Soc., 2008, 130: 3296
2. X. H. Chen, T. Wu, G. Wu, R. H. Liu, H. Chen, and D. F. Fang, Nature, 2008, 453: 761
3. G. F. Chen, Z. Li, D. Wu, W. Z. Hu, J. Dong, P. Zheng, J. L. Luo, and N. L. Wang, Phys. Rev. Lett., 2008, 100: 247002
4. C. de la Cruz, Q. Huang, J. W. Lynn, J. Li, W. Ratcliff, J. L. Zarestky, H. A. Mook, G. F. Chen, J. L. Luo, N. L. Wang, and P. Dai, Nature, 2008, 453: 899
5. J. Zhao, Q. Huang, C. de la Cruz, S. Li, J. W. Lynn, Y. Chen, M. A. Green, G. F. Chen, G. Li, Z. Li, J. L. Luo, N. L. Wang, and P. Dai, Nature Mater., 2008, 7: 953
6. Y. Chen, J. W. Lynn, J. Li, G. Li, G. F. Chen, J. L. Luo, N. L. Wang, P. Dai, C. de la Cruz, and H. A. Mook, Phys. Rev. B, 2008, 78: 064515
7. J. Zhao, Q. Huang, C. de la Cruz, J. W. Lynn, M. D. Lumsden, Z. A. Ren, J. Yang, X. Shen, X. Dong, Z. Zhao, and P. Dai, Phys. Rev. B, 2008, 78: 132504
8. S. A. J. Kimber, D. N. Argyriou, F. Yokaichiya, K. Habicht, S. Gerischer, T. Hansen, T. Chatterji, R. Klingeler, C. Hess, G. Behr, A. Kondrat, and B. Büchner, Phys. Rev. B, 2008, 78: 140503
9. Y. Kamihara, H. Hiramatsu, M. Hirano, R. Kawamura, H. Yanagi, T. Kamiya, and H. Hosono, J. Am. Chem. Soc., 2006, 128: 10012
10. E. M. Brüning, C. Krellner, M. Baenitz, A. Jesche, F. Steglich, and C. Geibel, Phys. Rev. Lett., 2008, 101: 117206
11. L. Pourovskii, V. Vildosola, S. Biermann, and A. Georges, Europhys. Lett., 2008, 84: 370006
12. J. Dai, J. X. Zhu, and Q. Si, Phys. Rev. B, 2009, 80: 020505(R)
13. H. Maeter, H. Luetkens, Y. G. Pashkevich, A. Kwadrin, R. Khasanov, A. Amato, A. A. Gusev, K. V. Lamonova, D. A. Chervinskii, R. Klingeler, C. Hess, G. Behr, B. Büchner,

and H. H. Klauss, 2009, arXiv: 0904.1563
14. C. de la Cruz, W. Z. Hu, S. Li, Q. Huang, J. W. Lynn, M. A. Green, G. F. Chen, N. L. Wang, H. A. Mook, Qimiao Si, and P. Dai, 2009, arXiv: 0907.2853
15. S. Chi, D. T. Adroja, T. Guidi, R. Bewley, S. Li, J. Zhao, J. W. Lynn, C. M. Brown, Y. Qiu, G. F. Chen, J. L. Luo, N. L. Wang, and P. Dai, Phys. Rev. Lett., 2008, 101: 217002
16. R. Sachidanandam, T. Yildirim, A. B. Harris, A. Aharony, and O. Entin-Wohlman, Phys. Rev. B, 1997, 56: 260
17. D. Petitgrand, S. V. Maleyev, P. Bourges, and A. S. Ivanov, Phys. Rev. B, 1999, 59: 1079
18. J. Zhao, D. T. Adroja, D. X. Yao, R. Bewley, S. Li, X. F. Wang, G. Wu, X. H. Chen, J. Hu, and P. Dai, Nature Phys., 2009, 5: 555
19. D. X. Yao, and E. W. Carlson, Phys. Rev. B, 2008, 78: 052507